2024 7th International Conference on Soft Robotics (RoboSoft)
San Diego, CA, USA. April 14-17, 2024

Position Control for a Soft Actuator With High Uncertainty and Hysteresis

Phuc D.H. Bui[1] and Joshua A. Schultz[2]

Abstract— **A soft inflatable actuator composed of low shore hardness elastomer with thin chamber walls will exhibit high nonlinearity and hysteresis in its motion. The nonlinearity is in the relation between pressure and volume which contains some unstable working zones where there is no one-to-one mapping. Hysteresis causes the actuator to follow different trajectories between the loading (inflating) and unloading (deflating) motions. This makes precise control of its position difficult. To cope with the nonlinearity, we design an adaptive super-twisting controller and account for the uncertain relation between volume and pressure in the control design by fitting a nonlinear function. To address hysteresis, we propose a method to force the tip of the actuator to converge to any reference position on the global deflating path. This method helps to eliminate the uncertainty in the position of the actuator's tip. The controller presented moves the actuator to the desired position in the shortest time with minimal chattering in the control actions. This control method has good performance which is demonstrated through empirical results.**

I. INTRODUCTION

Robots and actuators made of silicone rubber can retain their shapes and can resist high temperatures and caustic chemicals. They also have excellent flexibility, adaptability, and biocompatibility [1]. This is why the most common material used for soft robots is silicone rubber [2] [3] [4]. However, the most desirable property of silicone for robotics, its large elongations, make it difficult to control, as challenging nonlinear material behaviors emerge at these high strain rates.

The motions of pneumatic inflatable soft actuators and robots depend heavily on the chamber pressure and volume (P-V), which in turn depends on the material and thickness of the chamber walls. In [2], Marechal et al. provided a general view of the relationship between stress and strain of a set of soft materials. The stress-strain curves in their studies are all strictly monotonically increasing because the specimens used in the experiments had high thicknesses (3 mm). Although they are nonlinear, with these strain-stress relations control is manageable because there is a one-to-one mapping between pressure and volume, allowing the nonlinearity to be inverted. However, for thinner actuators made of low Shore hardness materials, the relations are not strictly monotonic, because at certain operating ranges, with a single pressure value, there will be two or more corresponding values of volume. This makes the actuators less straightforward to control, and the position control for the actuator must rely on the volume instead, which is not as readily measured as pressure given the deformations that can occur. In this study, we examine the motions that occur passing through this non-strictly-monotonic region through experiments with actuators composed of several low Shore hardness materials. We also propose a method to account for the behavior in the control design process.

Motions of pneumatic soft actuators often do not traverse the same trajectory during the loading and unloading phases. This behavior is known as hysteresis. These hysteresis loops become wider as the chamber walls of the soft actuator become thinner. The soft robotics literature only contains a few examples of studies on hysteresis. Hosovsky et al. [5] analyzed the hysteretic behavior of a two-DOF soft robotic arm. The hysteresis loop they present is between the pressure and the joint angle between two links. However, as this robot is composed of rigid links actuated by pneumatic muscle, their hysteresis result may be radically different compared to a completely soft pneumatic robot. Minh et al. [6] investigated the hysteresis between the force and length of a pneumatic artificial muscle but did not provide any control method. Abbasi at al. [7] and Liu at al. [8] designed cascade strategies for the dynamics control of soft pneumatic actuators with hysteresis compensation. Their soft actuators did the motions in a two-dimensional space and the hysteresis was between the input and output angles. In our paper, we confront the uncertainty in positioning a robot in $\mathbb{R}^3$ posed by hysteresis and propose a control method to track the desired position.

Due to the non-monotonic relation between the pressure and volume, and the hysteretic motion of the soft actuator, we selected the adaptive super-twisting sliding mode control (STW SMC) algorithm to deal with the nonlinearity and control the actuator's position. A first-order SMC was designed to control a soft actuator in the work of Xavier et al. [9]. However, because the soft actuator in their system is thicker and has higher shore hardness, they were not forced to confront the non-monotonic behavior. Furthermore, hysteresis was not addressed in that work. Our work addresses the challenges of hysteresis and non-monotonicity in the material by using STW SMC. It also has adaptive parameters to deal with uncertainty and disturbances. One of the significant advantages of the STW SMC over the traditional first-

This work is supported by the NSF grant No. 1935312 EFRI C3 SoRo: Between a Soft Robot and a Hard Place: Estimation and Control Algorithms that Exploit Soft Robots' Unique Abilities

[1]The author is with Department of Mechanical Engineering, The University of Tulsa, 800 S. Tucker Drive, Tulsa, OK 74104, US; and with Gadomski School of Engineering, Christian Brothers University, 650 E Pkwy S, Memphis, TN 38104, US. [2]The author is with Department of Mechanical Engineering, The University of Tulsa, 800 S. Tucker Drive, Tulsa, OK 74104, US. [1]dbui@cbu.edu, [2]joshua-schultz@utulsa.edu

2024 IEEE 7th International Conference on Soft Robotics (RoboSoft) | 979-8-3503-8181-8/24/$31.00 ©2024 IEEE | DOI: 10.1109/ROBOSOFT60065.2024.10521939

order SMC is that it can reduce chattering considerably, which helps to protect the pneumatic proportional valve from damage.

The soft actuator being controlled in this study is "Squishy" developed by Williamson, et al. [10], [11]. It is an inflatable elastomeric chamber made of Smooth-On Dragon Skin 10 silicone with a thickness of 1 mm. The soft actuator has a thin band of fabric embedded longitudinally to reinforce one side (see Fig. 1). When inflated pneumatically, the unreinforced side can undergo large strains while the fabric side maintains a constant length, causing the chamber to bend and turn at the same time. Because its undeformed shape is a circular arc and the placement of the fabric, the actuator performs a motion in $\mathbb{R}^3$ when inflated, using only a single chamber. While its trajectory remains fixed along an unchanging 3D path, this actuator possesses capabilities beyond the reach of 2D soft actuators. As a motivational example, in the figure, we show "Squishy" controlling a paddle for maneuvering a future floating soft robot on the surface of the water.

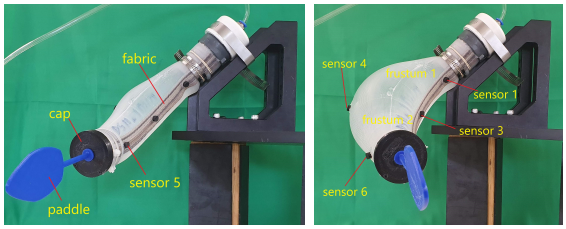

(a) At 2.5 kPa (b) At 4 kPa

Fig. 1. Dragon-Skin-10 actuator Squishy at low (a) and high (b) pressure

The rest of this paper is structured as follows. In Section II, we experimentally characterize the relation between the pressure and volume of the soft actuator. Section III discusses the hysteretic behavior of the actuator. Section IV describes the control design of the STW SMC. Section V presents the experimental evaluation of the proposed STW SMC methods. Section VI concludes the work.

II. Experimental Pressure-Volume Relations

Soft elastomeric materials often exhibit a nonlinear relationship between input and output. For latex rubber actuators, the Pressure-Volume (P-V) curve can have an unstable "N" shape with the first limit point and a second ascending branch or the upside-down "V" shape with a limit point for thin cylindrical tube shells, or a stable monotonic shape with thicker cylindrical tube shells [12]. The "N" shape in the behavior of a thin soft actuator can lead to a snap-buckling instability where minor perturbations in pressure rapidly change the actuator's volume within milliseconds [13].

Marechal et al. [2] characterized the input-output relations of a set of seventeen elastomers with shore hardness ranging from 00-10 to 40 A, through strain-stress curves of tensile tests conducted on 3 mm specimens. The experimental results in this work show that the lower hardness the elastomers have, the less steep their strain-stress curves are, but all the curves are stable monotonic. The results indicate that the P-V relations are repeatable when the material and thickness of the chambers are the same. However, the results from the work in [12] show that variation in thickness also affects the P-V relation of the latex rubber actuator. Hence, it is worth investigating whether silicone inflatable actuators with thinner chamber walls (less than 3 mm) will exhibit snap-through instability.

In the first part of this work, we conducted pressure-volume characterization experiments on thin-walled, low-shore-hardness silicone actuators to determine if they exhibit the snap-buckling instability observed in latex rubber actuators. The experiment was to see if the slicone actuators as seen in the behavior of. The silicone actuators include Dragon Skin 10 (shore hardness = 10 A), Ecoflex 00-10 (shore hardness = 00-10), and Dragon Skin FX Pro (shore hardness = 00-02). All actuators have the same shape and chamber thickness of 1 mm. Each actuator is a quarter-circle annulus with an inner radius of 105 mm and an outer radius of 147 mm. We placed 7 sensors of the electromagnetic motion tracking system (Polhemus Liberty) around the body of each actuator to measure its volume. Three sensors are along the fabric, at the black nodes in Fig. 1a, the other three are opposite to these first three, and the last one is at the center of the black cap. A fitting process involving a frustum of a cone was employed through Polhemus sensor values, targeting both the proximal (frustum 1) and distal (frustum 2) portions. These outcomes were then combined to yield the final volume measurement. For a visual representation of the sensor configuration, please refer to Fig. 2a. To validate the accuracy of our volume measurements using the Polhemus sensor, a series of controlled experiments were conducted using syringes to introduce predetermined volumes of water into the silicone chamber. To mitigate gravitational deformation, the actuator was positioned within a water tank to attain a neutral buoyancy. During each sampling instance, a consistent quantity of 50 ml of water was introduced and the corresponding volume was calculated based on Polhemus sensor data. The congruence between our calculated volume and the measured water volume is illustrated in Fig. 2b, affirming the precision of our measurement methodology. The coefficient of determination (R^2) is reported as 0.99, further validating the accuracy of our volume measurement technique.

When inflated with air, the chamber pressure was measured by the Honeywell pressure sensor SSCSANN001BGAA5 (range: 0 kPa - 100 kPa, resolution: 0.03 kPa). We inflated each actuator by repeating the following cycle until the volume of the actuator reached 1.2 l: opening the control valve to have the inflow at 0.01 l/s in 200 ms, then stopping for 5 seconds and recording the pressure and volume. The empirical P-V curves for each elastomer are shown in Fig. 3. This figure shows that while the latex rubber actuator has an unstable P-V curve, agreeing with the result in [12], the thin silicone actuators have monotonic but (not strictly monotonic) P-V curves with the same slope as those in [2]. Unlike the results

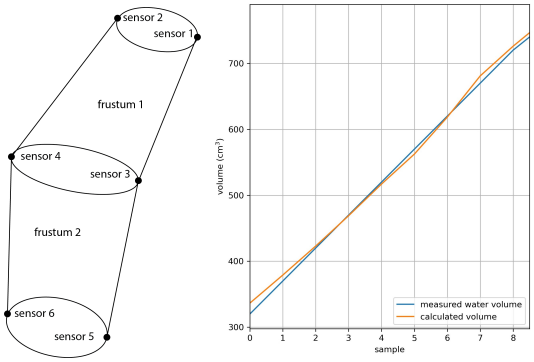

(a) The sensor configuration and the frustums (b) Correlation between the measured volume and the calculated volume

Fig. 2. The validation of volume measurement

of that work, the thin-walled chambers we studied have non-strictly monotonic P-V curves, including several ranges where the slope is zero. At these zones, the volume can increase with no commensurate increase in pressure. This behavior is marginally stable and makes the control of the actuator difficult; in this range, the tip position (which follows directly from chamber volume) can not be set by commanding the pressure, as the P-V relation is not one-to-one.

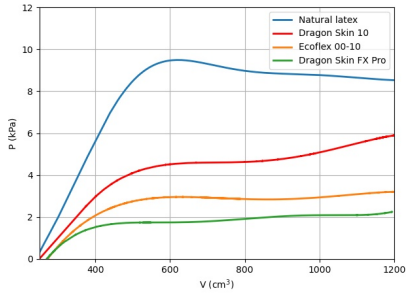

Fig. 3. Pressure-volume relations of actuators with 1 mm thickness and different SH. Note the nonlinearity above 400 cm^3.

III. Hysteresis Observed During Motion

Most soft actuators and robots exhibit not only nonlinear behaviors but also hysteresis. Hysteresis in soft actuators can cause poor tracking results and potential uncertainties [14]. Hysteresis is the phenomenon when a system traces different trajectories during loading vs. unloading. Regarding position control, the current output of the system depends not only on the current input but also on the history of the input. Hysteresis behavior is also unique to a specific system configuration [5].

We studied the hysteresis of our Dragon-Skin-10 actuator by measuring the trajectory of its tip in a motion cycle when it is inflated from 3.5 kPa (the lowest pressure that the actuator can stay stable under gravity) to 5 kPa (the highest pressure in its safety zone) and then deflated back to 3.5 kPa. The curve traced by the tip in $\mathbb{R}^3$ is illustrated in Fig. 4 with two views shown for better clarity. The green curve corresponds to inflation and will be referred to as the global "inflating" path hereafter. Similarly, the blue curve corresponds to deflation and will be referred to as the global "deflating" path hereafter. This hysteresis loop is called "global hysteresis" to distinguish it from the local hysteresis in cases where the actuator stops in the middle of the global hysteresis path. It can be observed that at the area near the head of the hysteresis (near the start and end points), the two paths diverge from each other and they converge when reaching the tail of the hysteretic loop. This behavior makes sense because the pressure is lower at the head of the hysteresis and higher at the other side. Given a desired position in space, how do we control the tip to a steady state position as it will have to traverse a hysteresis loop to get there? This problem will be solved in the next section.

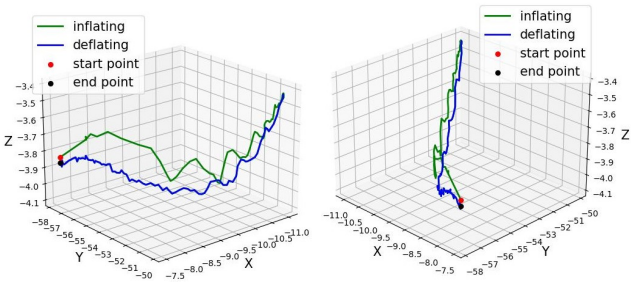

(a) Azimuth=50, Elevation=20 (b) Azimuth=-120, Elevation=5

Fig. 4. Hysteretic motion of the actuator

IV. Position Control Method for the Actuator

A. Pressure Dynamics of the Actuator

The controller is designed for the Dragon-Skin-10 actuator. The actuator is operated by providing a command to a proportion spool valve letting air into or out of the chamber. The chamber pressure depends on the net air flow given by the difference between the in and out flow rates. In our system, the in and out air flows are controlled by a 5/3 bidirectional proportional valve (Enfield LS-V15s) with a fast valve spool response (2.5 ms). The spool voice coil duty cycle is generated by an Arduino Uno with current provided by a Pololu driver (A4990) to control the opening of the valve. The compressed air supply is regulated by a regulator before entering the control valve. The outlet port of the valve is connected to the actuator chamber and the pressure sensor. The exhaust port is open to the atmosphere. The volume of the actuator is measured by 7 sensors of the Polhemus 3D motion tracking system. The thermodynamic process is considered to be isothermal with uniform gas temperature at all locations in the system.

The pressure dynamics of a pneumatic soft actuator have been well developed by Xavier et al. [9] and are summarized by the following differential equation:

$$\frac{dP}{dt} = \frac{P}{V}(Q_i - Q_o) \tag{1}$$

where P and V are the pressure and volume of the actuator. Q_i and Q_o air flow in and out given by:

$$Q_i = \frac{114.5 u_i C_v \sqrt{P(P_r - P)}}{\sqrt{T}} \tag{2}$$

$$Q_o = \frac{114.5 u_o C_v \sqrt{P_{atm}(P - P_{atm})}}{\sqrt{T}} \tag{3}$$

where P_r is the regulator pressure; P_{atm} is the atmospheric pressure; T is the system temperature; C_v is the flow coefficient of the control valve, and u_i and u_o are the duty cycles for the charging and discharging valves, respectively. Since we use one 5/3 proportional valve instead of two on/off valves for in and outflows, $u_i = u_o = u$.

Prior studies consider the volume V to be constant. Because our actuator has chamber walls that strain considerably, and as stated in Section II, V will vary. Furthermore, the relation between pressure and volume is non-strictly monotonic non-one-to-one mappings between the pressure and volume, and this may lead to instability in the control system if it is not considered carefully. It is also important to note that the characterization of the P-V relation of this class of thin soft actuators suggests designers control the position of their end effectors through volume rather than the pressure of the chamber. To account for the nonlinear P-V relationship in the control design, we fit a curve to the raw data of the Dragon-Skin-10 actuator. A cube root function is given in Eq. (4) (graphically illustrated in Fig. 5), showing the value of the volume V w.r.t pressure P fit the relationship well. This function and the original data have a R^2 square value as high as 0.98, indicating a high correlation between them.

$$V \approx a\sqrt[3]{(P+b)} + P + c \tag{4}$$

where the fitting parameters were determined empirically to be

$$a = 330, b = -4.65, c = 769.7 \tag{5}$$

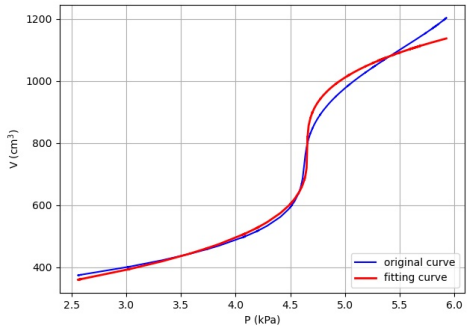

Fig. 5. Volume-pressure relation of the actuator and the fitting curve

B. Distance-Volume Relation Modeling

When inflated, the tip of the actuator traces out a parametric curve in $\mathbb{R}^3$. Therefore, we need to find a single variable that can represent the tip's position so we can describe a one-to-one mapping between this variable and the chamber volume. For this type of fabric-reinforced inflatable actuator, we observed that the distance S from the base of the actuator to its tip varies nearly linearly with volume. Furthermore, we also noticed that the actuator's tip can be forced to converge to any position along the global deflating path of the global hysteresis loop by conducting the motion appropriately, even when the actuator is inflating. This discovery allows us to bypass hysteresis issues by controlling the actuator to a steady state reference point that lies along this path. To accomplish this, we calculate the distance S for each point in space along the global deflating path of the global hysteretic loop described in Section III w.r.t the coordinate origin. The idea is illustrated in Fig. 6a where the green lines indicate the distances; to illustrate, the thicker green line depicts the distance from the origin to one selected reference point (red). It is worth noting that these distances are inversely proportional to the volume, as shown in Fig. 6b, because the coordinate system is set so that when the actuator bends further due to higher pressure (higher volume), the tip moves closer to the origin. We then can easily find a function to represent the linear $S - V$ relationship as:

$$S = mV + n \tag{6}$$

where

$$m = -1.08, n = 62.18 \tag{7}$$

Substituting V from Eq. 4 results in the following:

$$S = m\left(a\sqrt[3]{(P+b)} + P + c\right) + n \tag{8}$$

This linear fit and the raw data have a R^2 score up to 0.99. They are both plotted in Fig. 6b. Thus, we have a one-to-one mapping between the 3D position of the tip and the distance to the origin.

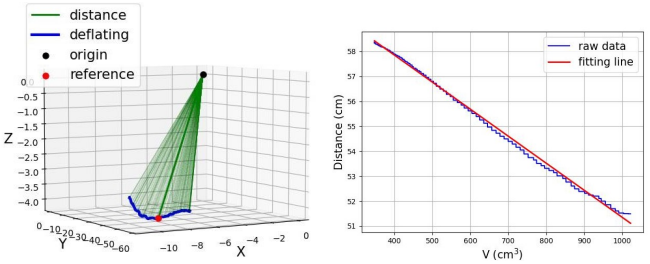

(a) Distances from the origin to each point in the deflating path (b) Distance-volume relation of the actuator

Fig. 6. Distance of the actuator's tip and the relation to its volume

C. Controller Design

Choosing our system state as $x = P$ in the pressure dynamics (1), it can be rewritten in the form of a general nonlinear dynamic system as:

$$\begin{aligned} \dot{x} &= f(x) + g(x)u \\ y(x) &= S(x) \end{aligned} \tag{9}$$

where S is the function showing distance-pressure relation in (8), and

$$f(x) = -\frac{114.5C_v}{V\sqrt{T}} x\sqrt{P_{atm}(x - P_{atm})} \tag{10}$$

$$g(x) = \frac{114.5C_v}{V\sqrt{T}} x\left(\sqrt{x(P_r - x)} + \sqrt{P_{atm}(x - P_{atm})}\right) \tag{11}$$

The control objective is to make the system output y track a desired value y_r, i.e. the output error variable $e = y_r - y$ tends to some small vicinity of zero. Because the dynamics system is first order, the sliding surface is chosen to be $s = \dot{e} + ke$, with k is a positive constant. The control problem is equivalent to driving the sliding variable s to zero. So the condition for the tracking problem is $\dot{e} + ke = 0$, which is equivalent to:

$$\dot{y_r} - \dot{y} + k(y_r - y) = 0 \tag{12}$$

Taking the derivative of y and substituting (8) and (9) into (12) results in:

$$\dot{y_r} - \left(\frac{ma}{(x+b)^{2/3}} + mf(x) + mg(x)u\right) + k(y_r - y) = 0 \tag{13}$$

From here the equivalent control law can be derived from the above equation:

$$u = \frac{1}{mg(x)}\left(\dot{y_r} - \frac{ma}{(x+b)^{2/3}} - mf(x) + k(y_r - y)\right) \tag{14}$$

The SMC is designed to have an equivalent part $u_{eq} = u$ and a switching part u_{sw} as:

$$U = u_{eq} + u_{sw} \tag{15}$$

for a traditional first-order SMC, the switching part includes a signum function that steers the system across the switching manifold; this causes chattering in control actions. Therefore, we applied the STW (second-order) SMC into the switching part to smoothen the control actions. The designed switching controller is based on the approach proposed by Shtessel et al. [15] and given as follows:

$$\begin{aligned} u_{sw} &= -\alpha\sqrt{|s|}\text{sgn}(s) + v \\ \dot{v} &= -\beta\text{sgn}(s) \end{aligned} \tag{16}$$

Here the control gains α and β are updated as follows:

$$\alpha = \begin{cases} \omega\sqrt{\gamma/2} & \text{if } |s| > \psi \\ 0 & \text{otherwise} \end{cases} \tag{17}$$

$$\beta = 2\epsilon\alpha + \lambda + 4\epsilon \tag{18}$$

where ω, γ, λ and ϵ are arbitrary positive constants and ψ is the chosen boundary for the sliding surface.

Since the control gains α and β are adaptable, this STW SMC can deal with uncertainties such as the one in V-P relation and disturbances. The selected control scheme also affords the control designer with additional parameters with which to tune the response by adjusting ω, γ, λ, and ϵ to tailor the motion characteristics including the rise time and overshoot of the system. These parameters provide more freedom in tuning the controller over the traditional SMC. Furthermore, STW SMC provides control actions with lower chattering than the traditional SMC to protect the control valve.

V. Experimental Control Results

To evaluate the control performance, we selected a representative reference point on the deflating path at point $A = (-9.48, -55.08, 4.06)$ to demonstrate that the STW SMC drives the actuator's tip to reach the 3D position whether inflating or deflating. This position corresponds to a distance of 56 cm from the origin. By adjusting the control parameters, we could control the actuator at three different speeds: high speed (2.33 cm/s), medium speed (1.88 cm/s), and low speed (0.92 cm/s), e.g., for the low-speed motion, the control parameters were selected as $k = 2$, $\psi = 2$, $\omega = 0.02$, $\gamma = 0.02$, $\lambda = 0.005$ and $\epsilon = 0.005$. The actuator's tracking performance at each speed is shown in Fig. 7. The first row of this figure shows the approach in $\mathbb{R}^3$ to the desired reference point. The second row displays the corresponding position tracking and the third row shows the position errors over time. When running at high speed (2.33 cm/s), we observed that the actuator tip traverses the first part of the inflating path rapidly before converging to the reference point (red). When running at medium speed (1.88 cm/s), the path of the tip falls in between the global inflating and deflating paths. When running at low speed (0.92 cm/s), the tip nearly follows the global deflating path on its way to the reference point. This indicates that the speed of the motion will affect the path through space the actuator tip will take. Our experiments also indicated that at high (2.33 cm/s) and medium (1.88 cm/s) speeds, unless the tip overshoots the desired location it will not converge to the reference point but will instead end up at some points in the inner zone between the inflating and deflating paths. This comports with our observation that when inflating at medium to high speeds, the tip has the tendency to trace a path that lies above the deflating path. In other words, our algorithm capitalizes on the actuator's system dynamics, utilizing overshoots to force the actuator through local hysteresis to reach the desired location. In general, the actuator tip can reach the reference point in one of two manners: by moving close to the deflation curve at a low speed to approach the reference point from an S value below the intended target or with medium to high speeds and using the overshoots to approach the reference point from an S value above the intended target.

We observed satisfactory convergence throughout the deflating curve, and we also show the position tracking at another reference point, $B = (-9.95, -53.9, -4.05)$, for completeness, in Fig. 8. This reference point corresponds to a distance of $S = 55$ cm from the origin. As with the prior reference point A, we can drive the actuator to converge to the desired point B along the global deflating path by designing the proper speed and overshoot, and this works in general.

In Fig. 9, we present the control signals obtained from both the traditional first-order SMC and the STW SMC. Each curve represents the fastest convergence we were able to achieve by tuning control parameters. These signals are derived under identical reference conditions and operating speeds. A clear distinction emerges upon inspection: the

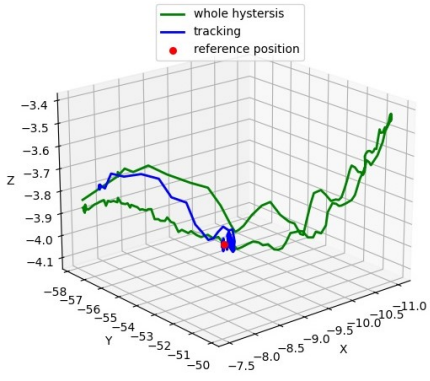

(a) Position tracking at high speed (2.33 cm/s)

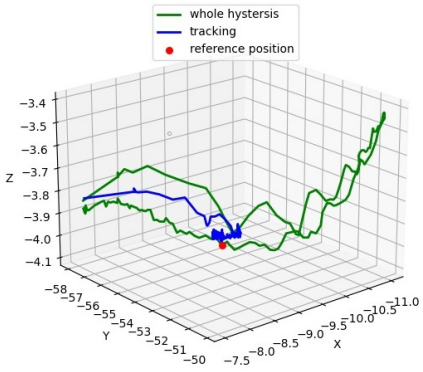

(b) Position tracking at medium speed (1.88 cm/s)

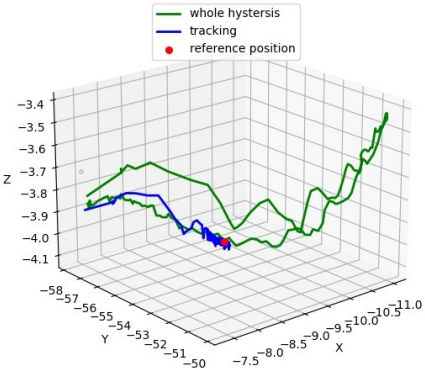

(c) Position tracking at low speed (0.92 cm/s)

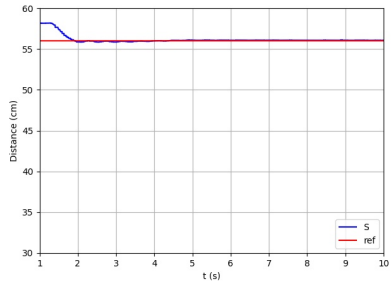

(d) Distance tracking at high speed (2.33 cm/s)

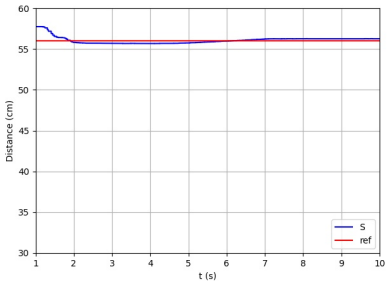

(e) Distance tracking at medium speed (1.88 cm/s)

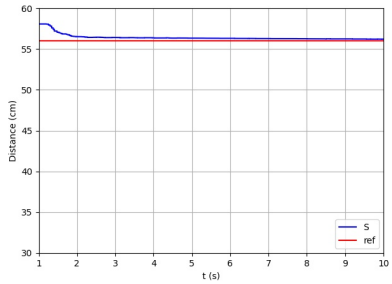

(f) Distance tracking at low speed (0.92 cm/s)

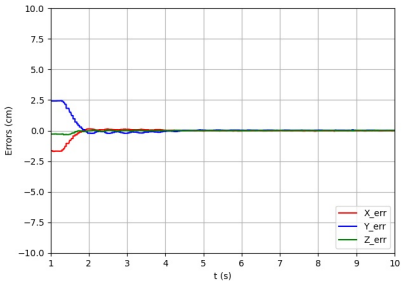

(g) Position error at high speed (2.33 cm/s)

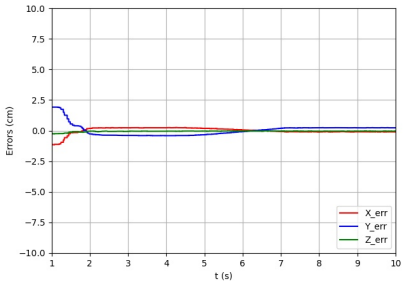

(h) Position error at medium speed (1.88 cm/s)

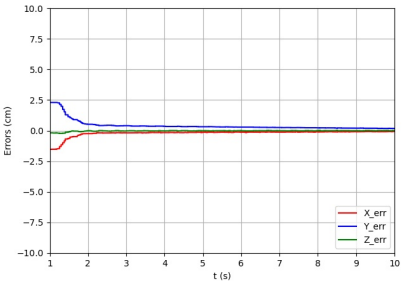

(i) Position error at low speed (0.92 cm/s)

Fig. 7. Control performance for tracking reference point A(-9.48,-55.08,4.06) at different speeds

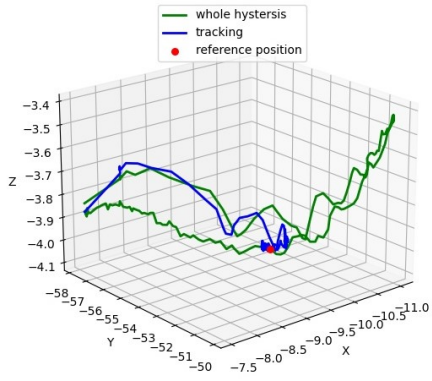

(a) Position tracking at high speed (2.33 cm/s)

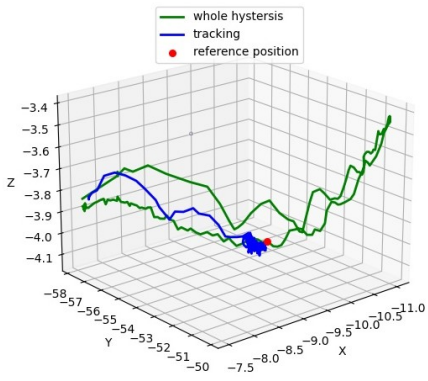

(b) Position tracking at medium speed (1.88 cm/s)

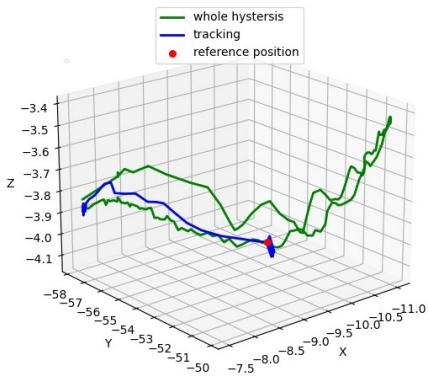

(c) Position tracking at low speed (0.92 cm/s)

Fig. 8. 3D position tracking reference point B(-9.95,-53.9,-4.05) at different speeds

STW SMC yields smoother control signals, while the first-order SMC exhibits more pronounced chattering. To quantify this difference, we analyzed the peak-to-peak variations in both control signals within each second, using a threshold of 0.5 for comparison.

The results show that the chattering level of the STW SMC control signal is measured at 20.74 %, while the first-order SMC registers a higher chattering level of 35.91 %. This indicates that the STW SMC control signal reduces chattering by a significant 15.17 % compared to the first-order SMC. We see that the additional tuning parameters of the STW SMC give us the ability to reduce the amount of chattering, resulting in a faster settling time. Such an improvement not only enhances the lifespan of the proportional valve but also contributes to substantial energy savings.

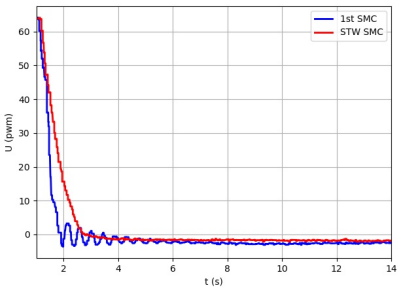

Fig. 9. The control signals of the first-order SMC and the STW SMC

VI. Conclusion

In this work, we conducted experiments that show that a soft actuator made of materials with low shore hardness and thickness has a relation between pressure and volume that is not strictly monotonic, unlike that observed with thicker-walled chambers with higher hardness. This complex relation creates a more challenging control structure for this class of soft actuators where commanding volume to reach a desired position is more effective than commanding chamber pressure. The motion of the soft actuator is subject to substantial hysteresis, which renders it challenging to do position control as the actuator's path will depend on the input direction. To deal with the uncertainty and hysteresis, we developed an empirical relation between position, distance to the origin, volume, and pressure; and designed an adaptive Super Twisting Sliding Mode Controller that allows us to force the tip of the actuator to converge to a desired reference position on the global deflating path. To do that, we tuned the Super Twisting control parameters so that the actuator can perform a motion at low speed or medium to high speeds while capitalizing on overshoot behavior. The additional tuning parameters provided by the Super Twisting Controller are instrumental to the success of the method. Experimental curves show that the control method successfully drives the actuator to reach a number of desired reference positions, overcoming $P-V$ uncertainty and hysteresis.

The single-chambered actuator has a single global inflation and deflation curve and as such the range of reference points in space that can be commanded is limited by the actuator architecture. Future work will explore combining the method with active materials embedded in the chamber wall to modulate these curves by activating these materials in various regions of the chamber wall, or using a multi-chambered embodiment. It would also be useful to examine the algorithm for cases in which the actuator encounters environmental forces other than gravity, such as during paddling a soft robotic surface craft.

References

[1] J. Li, S. Wu, W. Zhang, K. Ma, and G. Jin, "3D Printing of Silicone Elastomers for Soft Actuators," *Actuators*, vol. 11, p. 200, 7 2022.

[2] L. Marechal, P. Balland, L. Lindenroth, F. Petrou, C. Kontovounisios, and F. Bello, "Toward a Common Framework and Database of Materials for Soft Robotics," *Soft Rob.*, vol. 8(3), pp. 284–297, 2021.

[3] E. S. Keneth, A. Kamyshny, M. Totaro, L. Beccai, and S. Magdassi, "3D Printing Materials for Soft Robotics," *Advanced Materials*, vol. 33(19), p. 2003387, 5 2021.

[4] F. Schmitt, O. Piccin, L. Barbé, and B. Bayle, "Soft Robots Manufacturing: A Review," *Front. Robot. AI.*, vol. 5(2018), p. 00084, 7 2018.

[5] A. Hosovsky, J. Pitel, and K. Zidek, "Analysis of Hysteretic Behavior of Two-DOF soft Robotic Arm," *MMSJ*, vol. 2016, pp. 935–941, 9 2016.

[6] T. V. Minh, T. Tjahjowidodo, H. Ramon, and H. V. Brussel, "Non-local memory hysteresis in a pneumatic artificial muscle (PAM)," in *17th Mediterranean Conference on Control and Automation*, Thessaloniki, Greece, Jun-Jul 2009, pp. 640–645.

[7] P. Abbasi, M. A. Nekoui, M. Zareinejad, P. Abbasi, and Z. Azhang, "Position and force control of a soft pneumatic actuator," *Soft Rob.*, vol. 7(5), pp. 550–563, 2020.

[8] Z. Liu, X. Yin, K. Peng, X. Wang, and Q. Chen, "Soft pneumatic actuators adapted in multiple environments: A novel fuzzy cascade strategy for the dynamics control with hysteresis compensation," *Mechatronics*, vol. 84, p. 102797, 2022.

[9] M. S. Xavier, A. J. Fleming, and Y. K. Yong, "Model-Based Nonlinear Feedback Controllers for Pressure Control of Soft Pneumatic Actuators Using On/Off Valves," *Front. Robot. AI*, vol. 9, p. 818187, 3 2022.

[10] J. G. Williamson, C. Schell, M. Keller, and J. Schultz, "Extending the reach of single-chamber inflatable soft robots using Magnetorheological Fluids," in *IEEE International Conference on Soft Robotics*, New Haven, Connecticut, April 2021, pp. 119–125.

[11] P. D. H. Bui and J. Schultz, "A Semilinear Parameter-Varying Observer Method for Fabric Reinforced Soft Robots," *Front. Robot. AI*, vol. 8, p. 749591, 2021.

[12] A. Anssari-Benam, A. Bucchi, and G. Saccomandi, "Modelling the Inflation and Elastic Instabilities of Rubber-Like Spherical and Cylindrical Shells Using a New Generalised Neo-Hookean Strain Energy Function," *Journal of Elasticity*, vol. 151, pp. 15–45, 2022.

[13] R. Baumgartner, A. Kogler, J. M. Stadlbauer, C. C. Foo, and R. K. et al., "A Lesson from Plants: High-Speed Soft Robotic Actuators," *Adv. Sci.*, vol. 2020(7), p. 1903391, 2020.

[14] M. T. Thai, P. T. Phan, T. T. Hoang, H. Low, N. H. Lovell, and T. N. Do, "Design, Fabrication, and Hysteresis Modeling of Soft Microtubule Artificial Muscle (SMAM) for Medical Applications," *IEEE Robot. Autom.*, vol. 6(3), pp. 5089–5096, 7 2021.

[15] Y. Shtessel, J. Moreno, F. Plestan, L. Fridman, and A. Poznyak, "Super-twisting adaptive sliding mode control: a Lyapunov design," in *In 49th IEEE Conference on Decision and Control*, Atlanta, GA, USA, Dec 2010, pp. 5109–5113.